

The Nuclear Calcium Signaling Target, Activating Transcription Factor 3 (ATF3), Protects against Dendrotoxicity and Facilitates the Recovery of Synaptic Transmission after an Excitotoxic Insult*

Received for publication, January 1, 2014, and in revised form, February 4, 2014. Published, JBC Papers in Press, February 10, 2014, DOI 10.1074/jbc.M113.502914

Hanna Ahlgren[‡], Carlos Bas-Orth[‡], H. Ekehard Freitag[‡], Andrea Hellwig[‡], Ole Petter Ottersen[§], and Hilmar Bading^{‡1}

From the [‡]Department of Neurobiology, Interdisciplinary Center for Neurosciences, University of Heidelberg, INF 364, 69120 Heidelberg, Germany and the [§]Center for Molecular Biology and Neuroscience and Department of Anatomy, Institute of Basic Medical Sciences, University of Oslo, 0317 Oslo, Norway

Background: Injured neurons display dendritic beadings, which represent focal swellings of dendrites.

Results: Increased synaptic activity and overexpression of ATF3 reduce dendritic beading after an excitotoxic insult.

Conclusion: ATF3 overexpression facilitates recovery of neuronal network function after an excitotoxic insult.

Significance: ATF3-based dendroprotection promotes functional recovery after neuronal injury.

The focal swellings of dendrites (“dendritic beading”) are an early morphological hallmark of neuronal injury and dendrotoxicity. They are associated with a variety of pathological conditions, including brain ischemia, and cause an acute disruption of synaptic transmission and neuronal network function, which contribute to subsequent neuronal death. Here, we show that increased synaptic activity prior to excitotoxic injury protects, in a transcription-dependent manner, against dendritic beading. Expression of activating transcription factor 3 (ATF3), a nuclear calcium-regulated gene and member of the core gene program for acquired neuroprotection, can protect against dendritic beading. Conversely, knockdown of ATF3 exacerbates dendritic beading. Assessment of neuronal network functions using microelectrode array recordings revealed that hippocampal neurons expressing ATF3 were able to regain their ability for functional synaptic transmission and to participate in coherent neuronal network activity within 48 h after exposure to toxic concentrations of NMDA. Thus, in addition to attenuating cell death, synaptic activity and expression of ATF3 render hippocampal neurons more resistant to acute dendrotoxicity and loss of synapses. Dendroprotection can enhance recovery of neuronal network functions after excitotoxic insults.

In neuropathological conditions, such as brain ischemia, an excessive release of glutamate acting on *N*-methyl-D-aspartate receptors (NMDARs)² (1) causes loss of cellular energy and ion

homeostasis (2). This phenomenon, known as excitotoxicity (3), can induce both acute as well as delayed cell death (4). A key player in this process is the extrasynaptic NMDAR (eNMDAR), which, in contrast to the survival-promoting synaptic NMDAR (sNMDAR), initiates transcriptional shut-off and cell death pathways (5, 6). Dendrotoxicity is a hallmark of excitotoxicity that manifests as focal beading of the dendritic processes (7). Permanent dendritic beading in brain ischemia (8, 9) is associated with anoxic depolarization and is considered an early sign of acute injury in neurons often leading to neuronal cell death (10–12). In an *in vivo* model of brain ischemia, damaged dendrites in the core area show little or no recovery (13), whereas distant dendrites recover to some extent (10, 12, 14, 15). Neurons more distant to the injured area may undergo delayed death; they are the main targets of therapeutic interventions after neuronal injury.

In this study, we aimed at investigating whether the neuroprotective activity of the sNMDAR could shield hippocampal neurons against dendrotoxicity triggered by eNMDARs (5, 6). Neuroprotection is built up through a synaptic activity-driven process that involves the generation of nuclear calcium transients and induction of a cAMP-response element-binding protein (CREB)-dependent gene program for acquired neuroprotection (16–19). One of these so-called activity-regulated inhibitors of death genes (17) is the activating transcription factor 3 (*ATF3*). *ATF3* encodes for a transcriptional repressor; it is a direct target of nuclear calcium-CREB signaling and protects against eNMDAR-induced excitotoxicity as well as against oxygen-glucose deprivation *in vitro* and ischemic brain damage *in vivo* (20). Here, we show that increased synaptic activity protects, in a transcription-dependent manner, against dendritic beading. We further demonstrate that increasing the

response element-binding protein; EGFP, enhanced green fluorescent protein; MEA, microelectrode array; NLS, nuclear localization signal; rAAV, recombinant adeno-associated virus; TEM, transmission electron microscopy; DIV, days *in vitro*.

* This work was supported by the Letten Foundation (to H. A.), a European Research Council Advanced Grant (to H. B.), and Deutsche Forschungsgemeinschaft Grants SFB488 and SFB636.

¹ Member of the Excellence Cluster CellNetworks at Heidelberg University. To whom correspondence should be addressed: Dept. of Neurobiology, Interdisciplinary Center for Neurosciences, University of Heidelberg, INF 364, 69120 Heidelberg, Germany. E-mail: Hilmar.Bading@uni-hd.de.

² The abbreviations used are: NMDAR, *N*-methyl-D-aspartate receptor; eNMDAR, extrasynaptic NMDAR; sNMDAR, synaptic NMDAR; ATF3, activating transcription factor 3; AP, action potential; CaMBP4, calmodulin binding peptide 4; CaMK, calcium/calmodulin-dependent kinase; CREB, cAMP

levels of ATF3 in neurons renders neurons more resistant to dendrotoxicity and facilitates their ability to re-engage in synaptic transmission after an excitotoxic insult.

EXPERIMENTAL PROCEDURES

Hippocampal Cell Cultures—Hippocampal neurons from postnatal day 0 (p0) C57BL/6 mice were prepared and maintained as described previously (21) except that growth medium was supplemented with B27 (Invitrogen) and 1% rat serum. Neurons were plated either on poly-D-lysine/laminin-coated coverslips or in microelectrode array (MEA) dishes containing a grid of 60 planar electrodes (Multi Channel Systems) as described previously (22, 23). On day *in vitro* (DIV) 3, 2.4 μM cytosine D-arabinofuranoside (Sigma) was added to prevent proliferation of non-neuronal cells. On DIV8, growth medium was replaced with transfection medium (24), consisting of a salt/glucose/glycine solution and minimum Eagle's medium (9:1; v/v) plus sodium selenite 10 $\mu\text{g}/\text{ml}$, insulin 15 $\mu\text{g}/\text{ml}$, transferrin 8.25 $\mu\text{g}/\text{ml}$, and penicillin/streptomycin 0.5%. The salt/glucose/glycine solution contains the following (in mM): NaCl 114, NaHCO_3 26, KCl 5.3, MgCl_2 1, CaCl_2 2, HEPES 10, glycine 1, glucose 30, sodium pyruvate 0.5, phenol red 0.2%. All experiments were performed on DIV13–15 if not otherwise noted. The following chemicals were used: bicuculline (Enzo LifeScience); actinomycin D (Appllichem); 2-amino-5-phosphonovaleric acid and NMDA (Sigma); tetrodotoxin (Biotrend); dizocilpine (MK-801) (Tocris Bioscience), and Hoechst 33258 (Serva).

Plasmids and DNA Transfection—DNA plasmids used for transfections were enhanced green fluorescent protein (EGFP), under the control of an α -calcium/calmodulin-dependent protein kinase (α -CaMK) II promoter, mitochondrion-targeted mCherry, under the control of an α -CaMKII promoter (four tandem copies of the cytochrome *c* oxidase signal sequence (MSVLTPLLLRGLTGSARRLPVPRAKIHSLGDP) were fused to the N terminus of mCherry to ensure mitochondrial localization), an ATF3-FLAG expression vector containing a cytomegalovirus (CMV) enhancer/chicken β -actin hybrid promoter (17, 19), control knockdown plasmid expressing both EGFP, under the control of an α -CaMK II promoter, and a control shRNA (5'-CTACCGTTGTTATAGGTGTTGATATCCGCACCTATAACAACGGTAG-3'), under the control of a U6 polymerase III promoter, and an ATF3 knockdown plasmid expressing both EGFP, under the control of an α -CaMK II promoter, and an ATF3-specific shRNA (5'-TCCTAGCCTGTCAACATAATA-3') (17), under the control of a U6 polymerase III promoter. Hippocampal neuronal cultures were transfected 2–3 days prior to experiments using Lipofectamine 2000 (Invitrogen) as described (25). Co-transfection efficacy was 100% based on the percentage of neurons, which showed a co-localization of EGFP and FLAG after immunolabeling with the mouse anti-FLAG M2 monoclonal antibody (Sigma).

Recombinant Adeno-associated Viruses and Neuronal Infection—Vectors used for construction and packaging of adeno-associated viruses (rAAVs) have been described previously (17, 19, 26, 27). The rAAV vector for ATF3 contains a CMV/chicken β -actin hybrid promoter; ATF3 carries a FLAG

tag. The rAAV vector for mCherry-nuclear localization signal (NLS) expression carries a 1.3-kbp fragment of the mouse α -CaMKII promoter (27). The rAAV vector for mCherry-calmodulin (CaM)-binding peptide (CaMBP4)-NLS contains an α -CaMKII promoter (26). Infection efficiency (co-localization with Hoechst 33258) was \sim 80% for each of rAAV-mCherry-NLS, rAAV-mCherry-CaMBP4, and rAAV-ATF3-FLAG (determined with monoclonal anti-FLAG antibody). Viral particles were produced and purified as described previously (19, 27). Neuronal cultures were infected at DIV7. Co-transfection-infection efficacy was 80–90% and was determined by counting the percentage of neurons that showed co-localization of EGFP and anti-FLAG immunoreactivity or mCherry.

NMDA Toxicity Assay for Dendritic Beading and Cell Death—Hippocampal neurons grown on coverslips and transfected with EGFP were challenged for 10 min at 37 °C with different NMDA concentrations as follows (in μM): 2.5, 5, 10, 20, and 30. Stimulations were terminated by washing three times with transfection medium. After washout of NMDA, cells were either fixed immediately with 4% formaldehyde (freshly depolymerized from paraformaldehyde) supplemented with 4% sucrose or incubated for a further 2, 4, or 24 h at 37 °C before fixation. After fixation, nuclei were stained with Hoechst 33258 before mounting coverslips onto microscope slides using Mowiol. To increase synaptic activity, neurons were treated with 50 μM bicuculline for 15–16 h prior to an NMDA challenge. Bicuculline is a γ -amino butyric acid receptor type A blocker and induces recurrent synchronous network bursting (23). Bicuculline was dissolved in dimethyl sulfoxide (DMSO), and the final concentration of DMSO did not exceed 0.05%. Actinomycin D (10 $\mu\text{g}/\text{ml}$) was added 30 min prior to bicuculline stimulation. In the actinomycin D experiments and in the experiments with CaMBP4-infected neurons, bicuculline treatment was terminated by changing the media to transfection medium containing 1 μM tetrodotoxin 4 h before adding NMDA.

Assessment of Dendrite Morphology—Dendritic beading of hippocampal neurons was assessed immediately after NMDA stimulation or after a 2- or 4-h recovery period. An evaluation after a 24-h recovery period was not possible because most dendritic processes were virtually completely disintegrated. Dendritic beading was assessed by counting 15 EGFP-positive neurons for every coverslip (two coverslips per condition) for each experiment using a light microscope (Leica DM IRBE) with \times 40 magnification. Dendrites were classified as damaged if more than one spherical beading was detected within the dendritic arbor. Analysis was performed blindly. Data from one experiment (corresponding to hippocampal neurons from one preparation) were normalized to the minimum damage (*i.e.* the control group displaying the lowest number of EGFP-positive neurons with damaged dendrites under basal conditions) and maximum damage (*i.e.* the group displaying the highest number of EGFP-positive neurons with damaged dendrites after NMDA treatment). Statistical significance was assessed using one-way analysis of variance followed by Bonferroni's post hoc test. Data are presented as mean plus standard error of the mean (+ S.E.) from at least three independent experiments.

ATF3 Protects against Dendrotoxicity

Cell Death Analysis—Cell death was assessed immediately after NMDA stimulation or after a 24-h recovery period by the analysis of morphological abnormalities of the nuclei as described previously (5, 16, 17, 19, 20). The percentage of hippocampal neurons with condensed nuclei or large chromatin clumps was determined by counting Hoechst 33258-stained nuclei in 20 visual fields for every condition in each experiment at a light microscope (Leica DM IRBE) with 40 \times magnification.

Immunocytochemistry—Hippocampal neurons were fixed in 4% formaldehyde in phosphate-buffered saline (PBS) supplemented with 4% sucrose for 10–15 min at room temperature (RT) and were then permeabilized with Triton X-100 (0.3%) in PBS/Tween (0.1%) for 10–15 min. Neurons were subsequently incubated with 50 mM glycine, and nonspecific binding sites were blocked with PBS containing 2% bovine serum albumin (BSA) and 10% normal goat serum. Neurons were incubated overnight at 4 °C with primary antibodies. The following day, primary antibody was removed, and the neurons were washed repeatedly with PBS before incubation with secondary antibody for 45–60 min at RT. Finally, nuclei were stained with Hoechst 33258, and coverslips were mounted on microscope slides using Mowiol. The following antibodies were used in this study: mouse monoclonal anti-FLAG M2 antibody, 1:4000 (Sigma); rabbit polyclonal anti-ATF3, 1:400 (Santa Cruz Biotechnology, SC-188); goat anti-mouse Alexa 594, 1:750 (Invitrogen); and goat anti-rabbit Alexa 594, 1:500 (Invitrogen). Because ATF3 levels in resting neurons are very low and hard to detect by immunocytochemistry, cells were stimulated with 50 μ M bicuculline for 4 h before fixation for immunostaining of endogenous ATF3.

Confocal Imaging—Hippocampal neurons were imaged using a confocal laser-scanning microscope TCS SP2 (Leica) equipped with an inverted fluorescence microscope DM IRE2 (Leica) and Leica confocal scan software. For live imaging experiments, an HCX PL APO 63 \times 1.4 NA oil immersion objective (Leica) with 4 \times zoom was used. For all other confocal imaging experiments, an HCX PL APO 40 \times 1.25 NA oil immersion objective was used. All immunocytochemistry images were obtained with sequential acquisition settings at a resolution of 1024 \times 1024 pixels. Each image shown represents the z-stack projection of images taken at 0.5- μ m intervals. All live imaging experiments were performed at 22–24 °C. Hippocampal neurons plated on coverslips were transferred into a Ludin perfusion chamber (Life Imaging Services) connected to a peristaltic pump (Bio-Rad) with the perfusion speed adjusted to 1 ml/min. The chamber was filled with CO₂-independent salt/glucose/glycine solution ((in mM): NaCl 140.1, KCl 5.3, MgCl₂ 1, CaCl₂ 2, HEPES 10, glycine 1, glucose 30, and sodium pyruvate 0.5) (24) and mounted on the microscope stage. One EGFP-positive neuron was chosen per visible field, and z-stacks with optical sections of 0.3 μ m spanning the whole dendritic branch were collected every 5 min over a time period of 30 min. Time resolution of confocal live imaging was limited to 5 min to collect a z-stack of the dendritic arbor at each scanned time point. This was necessary to ensure the capture of dendritic structures, which change their focal plane during beading. EGFP was excited by a 488-nm laser line at 5–10% of maximal intensity, and emitted light was collected at 504–524 nm.

MCherry was excited by a 594-nm laser line at 15–25% of maximum intensity, and emission was collected at 600–620 nm. For EGFP and mCherry double-transfected cells, scans were made in parallel. All images were acquired at a resolution of 512 \times 512 pixels. The imaging protocol was as follows: 8 min baseline imaging, 10 min drug application, 12 min imaging after drug washout (including 5-min washings). Drugs, either NMDA solely or NMDA in the presence of MK-801 (20 μ M), were directly applied to the chamber with a pipette. NMDA sensitivity varies in hippocampal cell cultures between preparations (28) and was taken into account as we were investigating single cell responses. Inherent NMDA sensitivity was predetermined separately for each preparation on a control culture, and NMDA concentrations were then adjusted accordingly, typically to 20 μ M, to induce dendritic beading. Exposure for genetically manipulated neurons was the same as for control neurons. Images were saved as three-dimensional 8-bit TIFF files and converted to z-stack projections for data analysis. Forty- μ m dendritic segments on secondary or tertiary dendritic branches were outlined, and their area was measured with the open source software ImageJ at each time point collected. Measurements were normalized to the value obtained during baseline imaging. Statistical significance was assessed at each respective time point by repeated measure two-way analysis of variance followed by Bonferroni's post hoc test. Data are presented as mean + S.E. from three to six independent cell preparations.

Transmission Electron Microscopy (TEM)—Hippocampal neuronal cultures were challenged with NMDA (20 μ M) for 10 min at 37 °C. After washout of NMDA, neurons were fixed with 2% glutaraldehyde in 0.1 M sodium phosphate buffer, pH 7.4, and washed with 0.1 M sodium phosphate buffer. Neurons were post-fixed with 1% OsO₄, 1.5% K₄Fe(CN)₆, contrasted *en bloc* with uranyl acetate, dehydrated with a graded dilution series of ethanol, and embedded into glycid ether 100-based resin. Ultrathin sections were cut with a Reichert Ultracut S ultramicrotome (Leica Microsystems) and contrasted with uranyl acetate and lead citrate (29). Sections were examined in an electron microscope (Zeiss EM 10 CR) at an acceleration voltage of 60 kV. To obtain a quantitative measure of NMDA-induced rounding of mitochondria, TEM images of mitochondria located within intact dendrites (control) or within dendritic beadings (NMDA) were analyzed as follows. Using ImageJ software for each mitochondrion, the longest (*a*) and shortest (*b*) axis were measured, and the ratio *a/b* was calculated to determine a "form factor." A large form factor indicates an elongated morphology, whereas a form factor close to 1 indicates a rounded morphology. Only mitochondria that were located within longitudinally sectioned dendrites were included in the analysis.

Hippocampal Networks and MEA Recordings—MEA recordings were acquired with an MEA-60 amplifier board (10 Hz–35 kHz, gain 1200, sampling frequency 20 kHz, Multi-Channel Systems) as described previously (22, 23). The distance between the electrodes on the MEA dishes was 200 μ m and the electrode diameter was 30 μ m. Recordings of spontaneous network activity were acquired for 5 min once per day from DIV10 to DIV13. On DIV14, baseline network activity was recorded for 3 min

prior to NMDA application. Hippocampal neurons were treated for 10 min with 20 μM NMDA, which was washed out by changing the medium three times. Cultures were placed back into the incubator, and 3-min recordings were done at different time points (0.5, 1, 2, 4, 24, 48, and 72 h) after NMDA washout. Analysis was done with Neuroexplorer (NEX Technologies). RAAV-ATF3-FLAG culture values were compared with control culture values (noninfected and rAAV-mCherry-NLS) at each respective time point, and statistical significance was assessed by two-way analysis of variance followed by Bonferroni's post hoc test. Data are presented as mean + S.E. from four independent experiments.

RESULTS

Dendritic Beading and Changes in Neuronal Network Activity—The extent of dendritic beading and its reversibility in cortical and hippocampal preparations *in vitro* depends on the strength of the excitotoxic stimulus applied and on the age of the cultures (30–35). As a first step, we therefore determined, using cultured mouse hippocampal neurons at DIV14–15, the relationship between the NMDA concentration, and the degree of dendritic beading immediately following the insult, and the percentage of dead neurons 24 h after NMDA application. Hippocampal cultures were treated for 10 min with increasing concentrations of bath-applied NMDA and subjected to a morphological evaluation either immediately after the stimulation or following a recovery period of 2, 4, or 24 h. Cell death was assessed by analyzing the morphology of the cell nucleus stained with Hoechst 33258 (17, 19), and exogenously expressed EGFP was used to visualize dendritic beading in the form of focal dendritic beadings. NMDA bath application generated dendritic beading throughout the entire dendritic arbor (Fig. 1C). Low NMDA concentrations (2.5–10 μM) induced pronounced but transient dendritic beadings, which either partially or completely regressed during a 4-h recovery period. At higher NMDA concentrations (20–30 μM), the dendritic structure displayed little to no structural recovery (Fig. 1A). The cell death analysis revealed a similar dose-response pattern; at 24 h after NMDA bath application, we observed moderately elevated levels of cell death with 10 μM NMDA, which further increased with 20 and 30 μM NMDA (Fig. 1B).

Dendrites are the major postsynaptic structures for synaptic transmission, and dendritic beading has been shown to induce long lasting depression of synaptic transmission (31). To analyze the synaptic activity of a network of cultured hippocampal neurons, we performed MEA recordings (23). We found that bath application of 10 or 20 μM NMDA induced a short lived (~30 s) increase in the network firing rate (Fig. 1D). Cultures treated with 10 μM NMDA subsequently returned to activity levels slightly above control levels, whereas cultures treated with 20 μM NMDA progressed into a marked depression of network activity (Fig. 1D). During the 24-h recovery period following wash-out of NMDA, the activity levels of networks that had received 10 μM NMDA returned to levels similar to those measured in the controls. In contrast, in cultures treated with 20 μM NMDA, the firing rates remained suppressed (Fig. 1E). Thus, 10 μM NMDA bath application results in a slight increase in cell death and reversible dendritic beading, which allows for

a full recovery of a transient suppression of network activity. The use of 20 μM NMDA appears to be above threshold for inducing permanent dendritic beading that no longer permits a functional recovery of network activity and robustly increased cell death in our model system (Fig. 1, A, B, and E).

Excitotoxicity Is Associated with Morphological Changes of Dendrites and Mitochondria—An early ultrastructural change associated with acute neuronal damage is the rounding of mitochondria (36, 37), which under physiological conditions have an elongated morphology (36, 38). Mitochondrial rounding *in vitro* (36, 37) occurs within ~5 min after the onset of a prolonged depolarization and thus takes place at about the same time as dendritic beading *in vitro* (39) and *in vivo* (13, 40). To further characterize the temporal sequence of morphological alterations during acute neuronal damage in dissociated hippocampal cultures, we used confocal live time-lapse imaging and electron microscopy (EM). For simultaneous live imaging of dendrites and mitochondria, hippocampal neurons were cotransfected with plasmids containing expression cassettes for EGFP and a mitochondrially targeted mCherry. Imaging was performed according to the time scheme shown in Fig. 2A. We observed that dendritic beading and mitochondrial rounding appeared 2–7 min after NMDA application (Fig. 2B). Dendritic beadings generally exhibited a strong EGFP signal but occasionally lacked EGFP fluorescence and overlapped with mitochondrial structures; the structures linking the beads appeared as thin EGFP-positive strings (Fig. 2B). EM studies revealed more detailed information related to the dendritic ultrastructure before and 10 min after NMDA bath application (Fig. 2D). Neurons in the control group had dendrites with intact mitochondria, microtubules, and endoplasmic reticulum. Neurons treated with NMDA showed focal beadings on dendrites. Dendritic focal beadings were predominantly structures with low electron density; however, some beadings contained swollen endoplasmic reticulum as well as microtubules that appeared to have lost their continuity at the sites of the beadings. Mitochondria within beadings consistently showed a rounded morphology and damaged cristae (Fig. 2, D and E). Morphological alterations of mitochondria were specific to beadings and did not occur, for example, in pre-synaptic terminals in the same cultures (Fig. 2D). The structures between the beadings were void of larger organelles, consisting largely of tightly packed microtubules and other filaments. Similar microtubule-dense string-like dendritic structures linking the beads have been described at the ultrastructural level in hippocampal area CA1 in an *in vivo* model of brain ischemia (41). Pre-synaptic terminals in NMDA-treated cultures were morphologically similar to those in the control group.

In vitro, morphological alterations of both dendrites and mitochondria are considered to be initiated by NMDAR-mediated prolonged depolarization (34, 36, 42). Therefore, we challenged the cultures with NMDA in the presence of the NMDAR open channel blocker, MK-801 (20 μM). We found that both dendritic beading and mitochondrial rounding were blocked by MK-801 (Fig. 2C). During live imaging, we encountered an unexpected quenching of the EGFP signal during NMDA treatment (Fig. 2B) that abated after NMDA washout, particularly at focal dendritic beadings. Similar observations

ATF3 Protects against Dendrotoxicity

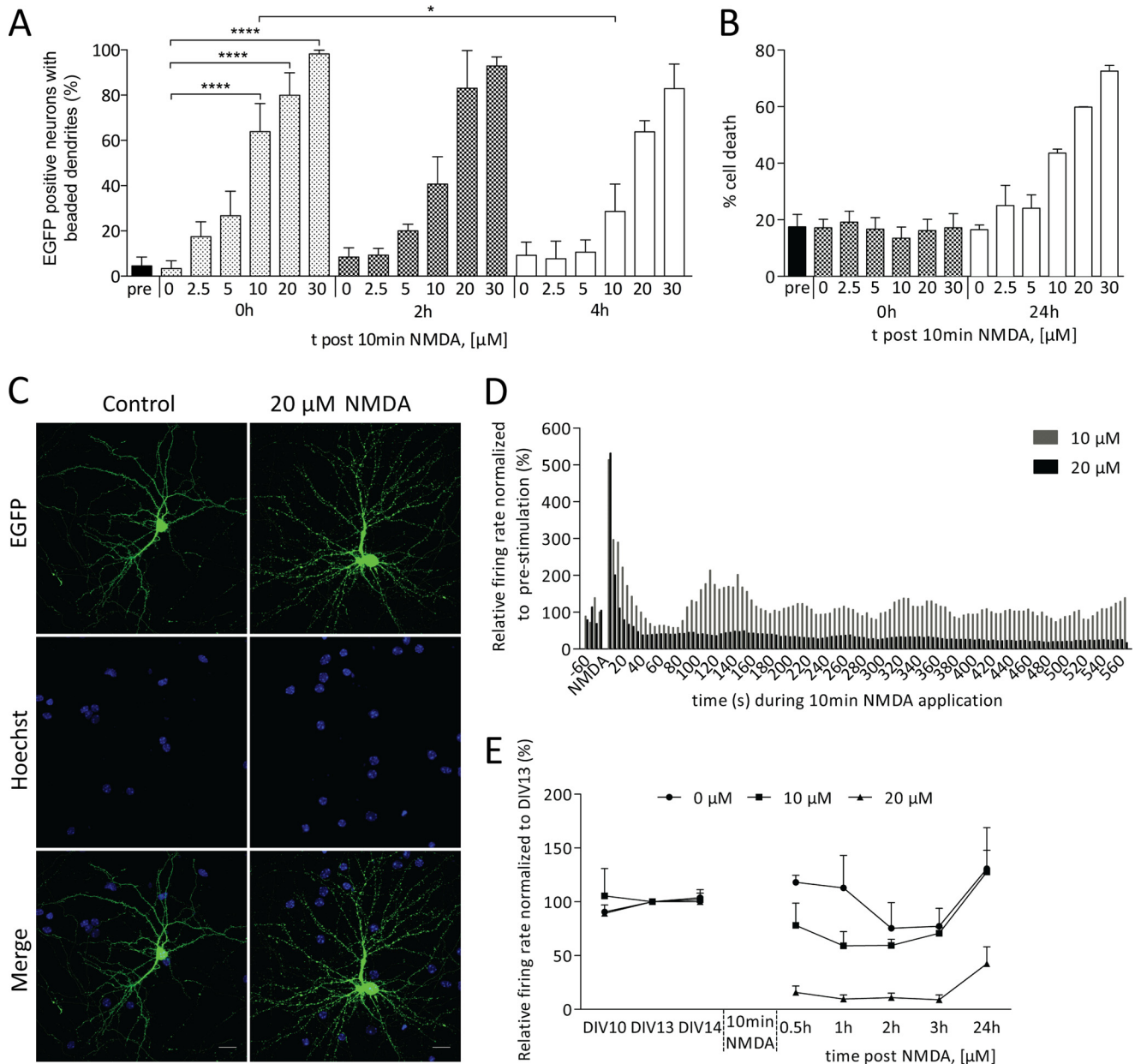


FIGURE 1. Dendritic beading, cell death, and neuronal network dysfunction induced by excitotoxic stimuli. A–C, dissociated mouse hippocampal cultures at DIV14–15 were challenged with 2.5, 5, 10, 20, or 30 μM NMDA for 10 min and fixed for morphological evaluation after a recovery period of 0, 2, or 4 h (dendritic morphology for beading) or 24 h (nuclear morphology for cell death). Neuronal cultures were transfected with an EGFP expression construct for individual cell visualization, and nuclei were counterstained with Hoechst 33258 for cell death analysis. Cell death and dendritic beading were evaluated based on morphological alterations (for details see “Experimental Procedures”). A, dose-response analysis of NMDA-induced dendritic beading presented as a percentage of EGFP-positive neurons. Statistically significant differences compared with 0 μM NMDA at 0 h are indicated with asterisks as follows: *, $p < 0.05$; ****, $p < 0.0001$. Columns represent mean + S.E. B, dose-response analysis of NMDA-induced cell death as a percentage of whole cell population. Representative images are presented of hippocampal neurons expressing EGFP before and 10 min after 20 μM NMDA bath application. C, scale bars, 20 μm . D and E, MEA analysis of network activity before and after application to 10–20 μM NMDA. Traces shown are representative of an acute response to a 10-min NMDA bath application (D). E, synaptic transmission measured 0.5 to 24 h after a 10-min exposure to 10 or 20 μM NMDA or to a control solution.

have been reported previously (39, 43). For this reason, it was not possible to analyze the spine structure during the initial stages of excitotoxic damage. Taken together, NMDA exposure of dissociated hippocampal cultures produces dendritic beading and ultrastructural changes that resemble toxicity associated morphological alterations observed *in vivo*. Dissociated hippocampal neurons are therefore a suitable model system for investigating mechanisms that protect against dendrotoxicity.

Synaptic Activity Protects against Acute Excitotoxic Damage—Increased neuronal activity and activation of sNMDARs have a protective effect against various toxic stimuli, including excitotoxicity (5, 16, 19, 26, 44, 45). We therefore investigated the possibility that increased synaptic activity before NMDA treatment could protect against dendrotoxicity. sNMDAR activity was increased by treating hippocampal neurons with the GABA_A receptor antagonist bicuculline (50 μM), which removes the inhibition from the neuronal network and

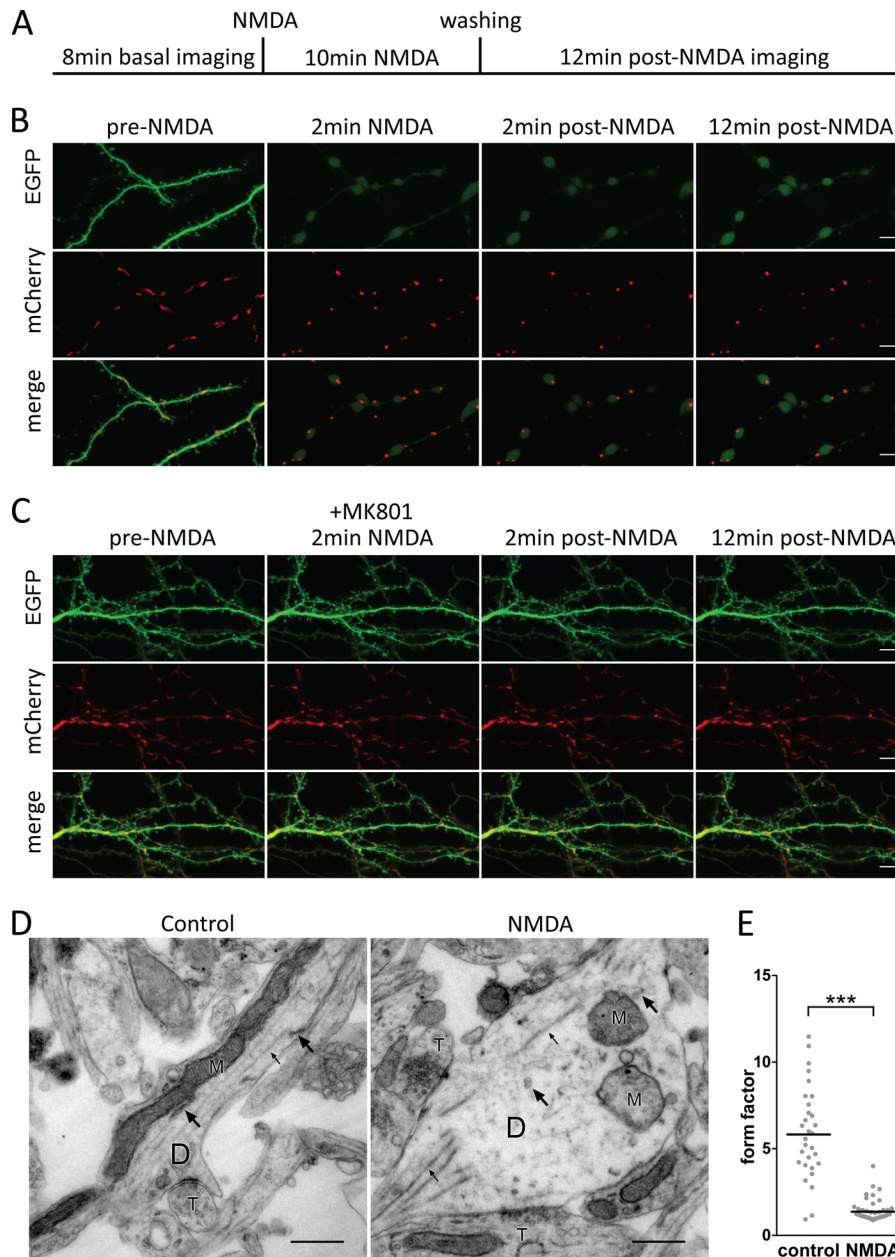


FIGURE 2. Rapid structural changes in hippocampal neurons in response to an excitotoxic insult. A–C, confocal live time-lapse imaging of hippocampal neurons expressing EGFP and mitochondrially targeted mCherry. The protocol used for live imaging is shown (A). Images are single plane projections of z-stacks at the indicated times before, during, and after washout of a 10-min NMDA ($20 \mu\text{M}$) application. Scale bars, $5 \mu\text{m}$ (B). C, data are the same as shown in B except that the NMDAR open-channel blocker MK-801 ($20 \mu\text{M}$) was included. D and E, TEM analysis of cultured hippocampal neurons; representative images are shown in D. Left panel, dendritic segment of a control neuron. Right panel, a swollen dendritic segment of a hippocampal neuron treated for 10 min with $20 \mu\text{M}$ NMDA (D, dendrite; M, mitochondrion; T, pre-synaptic terminal; small arrows indicate microtubules, large arrows indicate endoplasmic reticulum). Scale bars, $0.5 \mu\text{m}$. E, quantitative assessment of mitochondrial rounding using TEM images. A large form factor indicates an elongated morphology, whereas a form factor close to 1 indicates a rounded morphology (see “Experimental Procedures” for details). Graph illustrates individual numbers and mean for each group; $n = 31$ mitochondria (control) and $n = 53$ mitochondria (NMDA) from $n = 2$ experiments. Statistical significance was determined by unpaired two-tailed *t* test based on n and is indicated with asterisks; ***, $p < 0.001$.

leads to the generation of bursts of action potentials (AP). AP bursting in turn leads to an increase in the cytoplasmic and nuclear calcium concentrations (5, 23). Bicuculline treatment induced an enlargement of the dendritic spines (Fig. 3A), an indication of synaptic plasticity due to increased synaptic activity (46). Following 16 h of AP bursting, neurons were challenged with $20 \mu\text{M}$ NMDA for 10 min and immediately fixed for morphological evaluation. We found that in cultures pretreated for 16 h with bicuculline, the number of

EGFP-positive neurons with beaded dendrites was significantly reduced compared with nontreated cultures (Fig. 3B). These results indicate that increased synaptic activity offers protection against acute dendritic beading.

Activity-dependent Protection against Dendrotoxicity Is Dependent on Gene Transcription—Synaptic activity-mediated long lasting neuroprotection requires gene transcription (5, 16, 19). We therefore investigated the possibility that AP bursting-induced dendritic protection depends on synaptic activity-reg-

ATF3 Protects against Dendrotoxicity

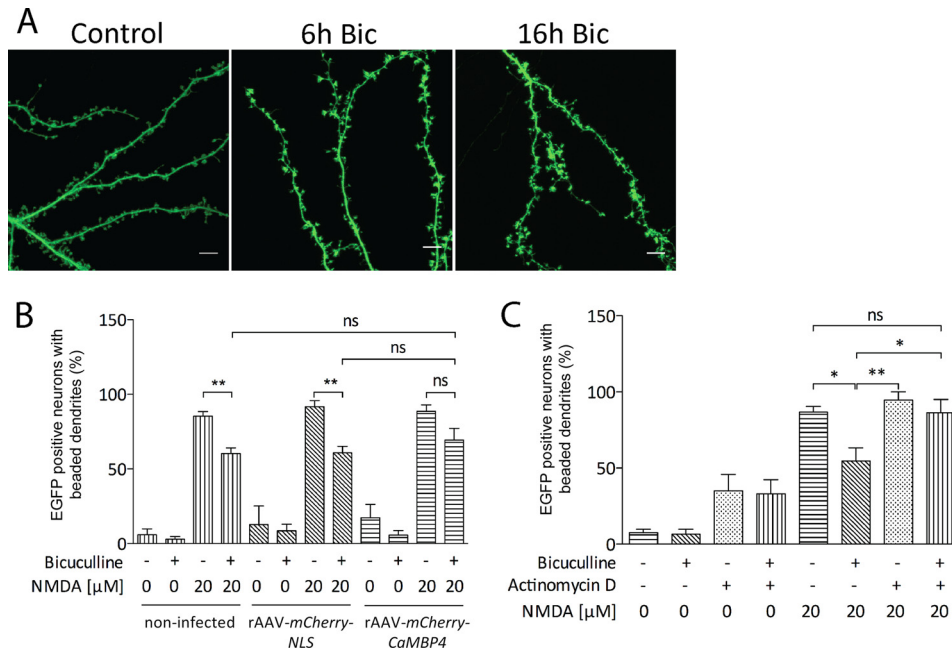


FIGURE 3. Synaptic activity protects against dendrotoxicity. *A*, representative confocal images of dendrites with spines of EGFP-transfected neurons subjected to 6 or 16 h of AP bursting induced by bicuculline (*Bic*) (50 μM). *Scale bars*, 5 μm . *B* and *C*, *histograms* show the quantification of the percentage of EGFP-positive neurons displaying dendritic beading after various treatments. *B*, 16 h of AP bursting induced by *Bic* reduces dendritic beading induced by a subsequent exposure to 20 μM NMDA for 10 min. Analysis of the role of nuclear calcium signaling for AP bursting mediated protection against NMDA-induced dendritic beading. Nuclear calcium signaling was blocked by infecting hippocampal neurons at DIV7 with rAAV-mCherry-CaMBP4 or, as control, with rAAV-mCherry-NLS. Cells were subsequently transfected with EGFP for visual assessment of dendritic beading (*B*). Analysis of the importance of transcription for AP bursting mediated protection against NMDA-induced dendritic beading. Transcription was blocked by actinomycin D (10 $\mu\text{g}/\text{ml}$) incubation prior to the induction of AP bursting (*C*). Tetrodotoxin (1 μM) was included in experiments with CaMBP4 and actinomycin D (*B* and *C*) during NMDA application to prevent secondary AP-mediated glutamate release. Statistically significant differences are indicated with asterisks as follows: *, $p < 0.05$; **, $p < 0.01$, ns = nonsignificant. *Columns* represent mean + S.E.

ulated gene expression by blocking gene transcription during bicuculline treatment with actinomycin D. We observed that the protective effect against NMDA-induced dendritic beading afforded by a 16-h period of AP bursting was abrogated by the blockade of gene transcription (Fig. 3C), indicating that the establishment of a protective shield against dendrotoxicity by synaptic activity requires a transcriptional response. However, blocking gene transcription for 16 h with actinomycin D also increased the amount of damaged dendrites in control cultures, which compromises the interpretation of these results. We therefore chose additional approaches to determine the transcription dependence of this form of neuroprotection. Because many AP bursting-induced transcriptional responses require an increase in the intranuclear calcium concentration (5, 16, 19), we investigated the role of nuclear calcium signaling in AP bursting-induced protection against dendritic beading. Nuclear calcium-regulated events were blocked in hippocampal neurons by expression of CaMBP4 (16, 17, 19), a nuclear protein that consists of four repeats of the M13 CaM-binding peptide derived from the myosin light chain kinase; it binds to and inactivates the nuclear calcium/CaM complex (47). We found that, in hippocampal neurons infected with rAAV-mCherry-CaMBP4, the AP bursting-induced protection was moderately but statistically not significantly smaller than the protection observed in uninfected and control-infected (rAAV-mCherry-NLS) hippocampal neurons (Fig. 3B). The lack of detection of a statistically significant inhibition of the synaptic activity-induced protection against dendrotoxicity by CaMBP4 may be due to residual activation of nuclear calcium-regulated neuroprotec-

tive genes. We therefore analyzed, using gain-of-function experiments, the potential of the nuclear calcium-regulated gene *ATF3* to shield against dendrotoxicity.

Overexpression of ATF3 Offers Protection against Dendrotoxicity—Activity-regulated inhibitors of death genes can protect neurons from cell death (17). Among the activity-regulated inhibitors of death genes is the nuclear calcium-regulated gene *ATF3* (17), which confers neuroprotection both *in vivo* and *in vitro* (20) but also enhances neuronal elongation and proliferation after a nerve injury (48, 49). To investigate a possible role of *ATF3* in dendrotoxicity, we first used confocal live time-lapse imaging to monitor structural alterations of the dendrites at various times after exposure of the neurons to NMDA. Hippocampal neurons were transfected with a plasmid containing an expression cassette for FLAG-tagged *ATF3*, which localized to the nucleus (Fig. 4A), alongside a plasmid containing an expression cassette for EGFP to label the dendrites for morphological analysis. We observed during live imaging that *ATF3*-overexpressing neurons were protected against an excitotoxic challenge (Fig. 4B). To quantify dendritic beading, the area of a 40- μm segment of a secondary or tertiary branch dendrite was measured at each time point after NMDA exposure. We found that the increase in dendritic area after NMDA application, which indicates the degree of beading, was far smaller in *ATF3*-overexpressing neurons compared with the control group (expressing EGFP only) (Fig. 4C). These results indicate that overexpression of *ATF3* renders hippocampal neurons more resistant against excitotoxic damage of dendrites.

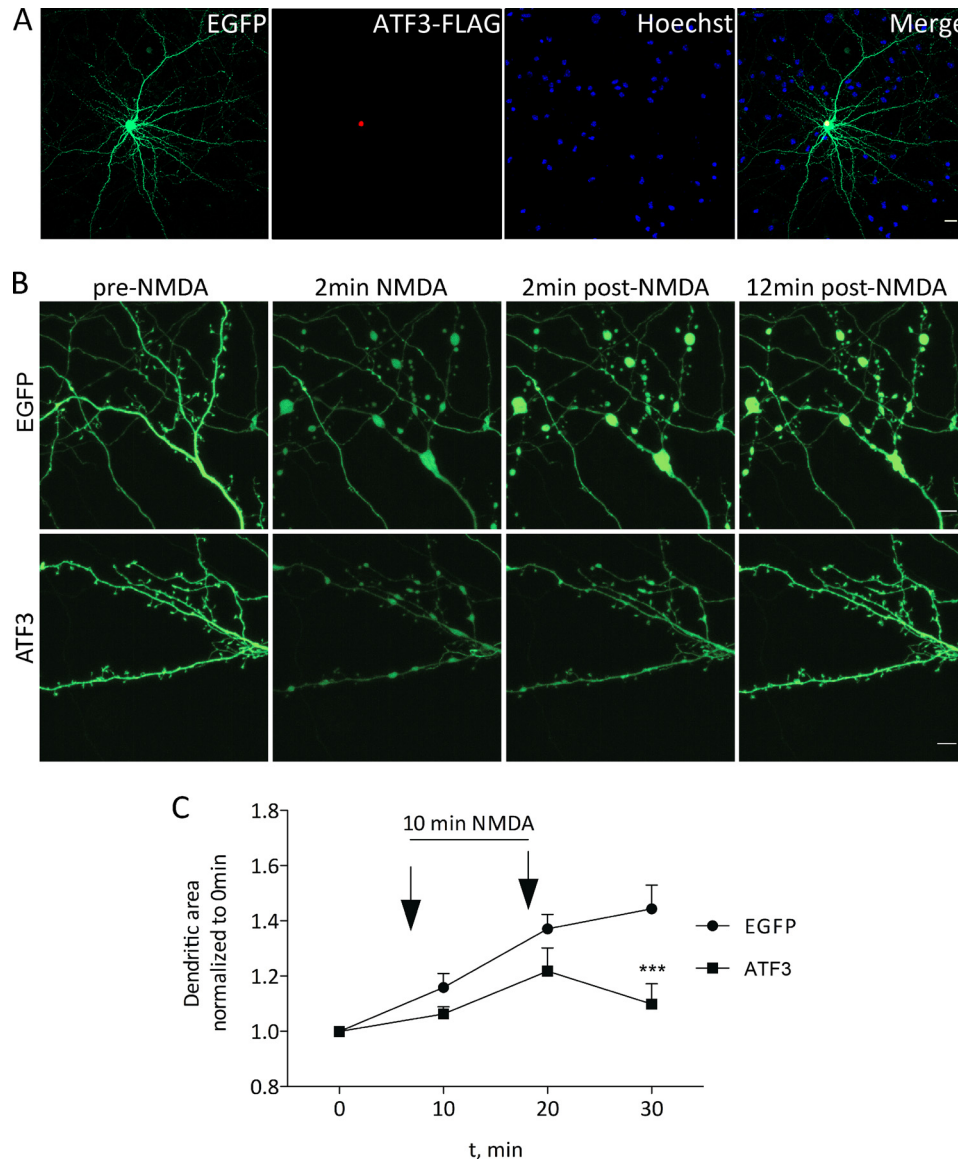


FIGURE 4. ATF3 is dendroprotective. *A* and *B*, confocal images (z-stacks projected into one plane) of cultured hippocampal neurons expressing FLAG-tagged ATF3 and EGFP at DIV11–12. A representative example is shown. Scale bar, 20 μ m (*A*). Confocal images showing dendritic beading of an ATF3-overexpressing and a control neuron at the indicated times before and after a 10-min application of 20 μ M NMDA. Scale bars, 1 μ m (*B*). *C*, quantification of dendritic area of ATF3-overexpressing and control neurons at the indicated time points after NMDA treatment. Statistically significant differences are indicated with asterisks as follows: ***, $p < 0.001$. Data are presented as mean + S.E.

ATF3 Loss of Function Exacerbates Dendrotoxicity—To provide further evidence for a role of ATF3 in protection against dendrotoxicity, we performed loss-of-function experiments. Neurons were transfected on DIV11 with dual expression plasmids that express EGFP and a short hairpin RNA (shRNA). Experiments were done on DIV13. We used immunostaining against endogenous ATF3 to validate the efficiency of our knockdown plasmid (Fig. 5, *A* and *B*). Live imaging revealed that NMDA-induced dendritic beading was more pronounced in neurons transfected with anti-ATF3 shRNA compared with control-transfected neurons (Fig. 5*C*). These findings indicate that loss of endogenous ATF3 enhances excitotoxic damage of dendrites.

Dendrites Protected by ATF3 Regain Their Ability to Participate in Synaptic Transmission—An important aspect of post-damage recovery of neuronal dendrites is the re-establishment

of synaptic connections and functional neuronal networks. We therefore investigated whether dendrites protected by ATF3 overexpression regained their ability to participate in synaptic transmission after an excitotoxic challenge. Hippocampal neurons plated on MEAs for recordings of population network activity were infected at DIV7 with either rAAV-ATF3-FLAG or with rAAV-mCherry-NLS. The infection efficiency determined immunocytochemically with anti-FLAG antibody was about 80% (Fig. 6*A*). Neuronal network activity was recorded before NMDA exposure (*i.e.* on DIV10–13) and at various times after the excitotoxic challenge that took place on DIV14. We found that both in control networks of uninfected or rAAV-mCherry-NLS-infected neurons as well as in networks of ATF3-overexpressing hippocampal neurons, a 10-min exposure to NMDA causes a prolonged suppression of firing lasting several hours (Fig. 6*B*). However, in contrast to the controls,

ATF3 Protects against Dendrotoxicity

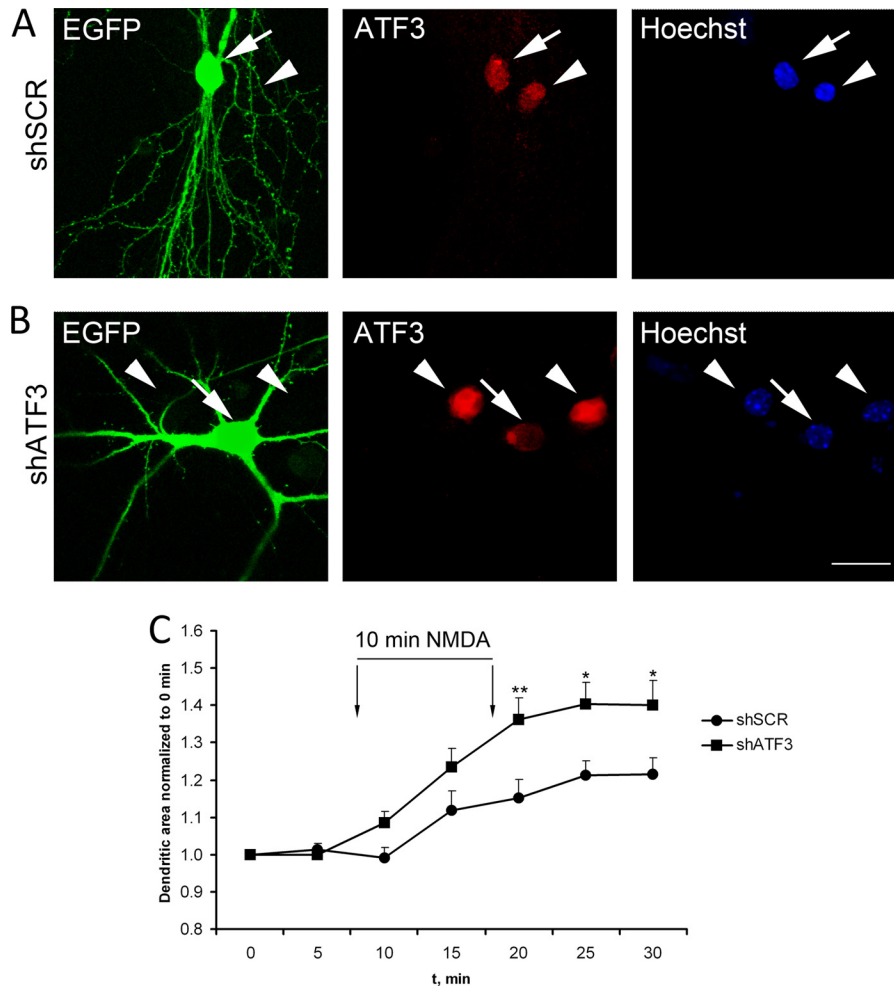


FIGURE 5. ATF3 loss-of-function renders neurons more susceptible to dendrotoxicity. *A* and *B*, confocal images (z-stacks projected into one plane) of cultured hippocampal neurons transfected with scrambled control shRNA (*shSCR*) (*A*) or ATF3 targeting shRNA (*shATF3*) (*B*). Transfected neurons are indicated with *arrows*, and untransfected neurons are indicated with *arrowheads*. The expression of endogenous ATF3 was detected immunocytochemically. *Scale bar*, 20 μm . *C*, quantification of dendritic area of ATF3 knockdown and control neurons at the indicated time points after NMDA treatment. Statistically significant differences are indicated with *asterisks* as follows: *, $p < 0.05$; **, $p < 0.01$. Data are presented as mean + S.E.

networks of ATF3-overexpressing neurons were able to regain their activity and after 48–72 h reached relative firing rates similar to those measured before the excitotoxic insult (Fig. 6*B*). These findings indicate that ATF3 not only helps to preserve an intact morphology of the dendritic tree after NMDA exposure (see Fig. 4) but that it also enhances the ability of neurons to recover synaptic connections and reestablish functional networks after an excitotoxic insult.

DISCUSSION

Over 3 decades ago, Olney *et al.* (7) described dendritic focal beading as one of the early hallmarks of neuronal damage in response to intraperitoneal kainate injections. This form of dendritic beading is considered to be one of the first ultrastructural changes in pathophysiological conditions (8, 50). Indeed, dendritic beading is linked both to ischemic depolarization and to excitotoxicity (4) and is considered to make neurons more susceptible to delayed cell death (41, 51). Targeting the processes underlying dendritic beading could be a strategy for preventing injury-associated network dysfunction and neuron loss. Here, we show that increased synaptic activity offers pro-

tection against dendritic beading. Our data indicate that this protection is gene transcription-dependent and that expression of ATF3, a synaptic activity and nuclear calcium-regulated gene, offers protection against dendrotoxicity induced by excitotoxic insults. Moreover, ATF3 enhances the functional recovery of synaptic transmission after dendritic beading.

Dendritic Beading Compromises the Function of Postsynaptic Compartments after Excitotoxic Damage, a Possible Role of an Excessive Water Influx—Electron microscopic analysis showed that after a toxic NMDA stimulus, the initial neuronal damage was only found in dendrites, whereas axonal terminals remained intact. These findings suggest that morphological changes specifically in the postsynaptic structures render neurons nonfunctional within their networks. Among the morphological changes induced by toxic NMDA exposure was a loss of microtubule continuity, which compromises the structural integrity of the dendrite, but likely also impairs microtubule-supported transport causing neuronal dysfunction. Microtubules disassemble when intracellular calcium concentrations increase to the micromolar range (52). Although calpain can cleave microtubules, this calcium-activated protease is unlikely

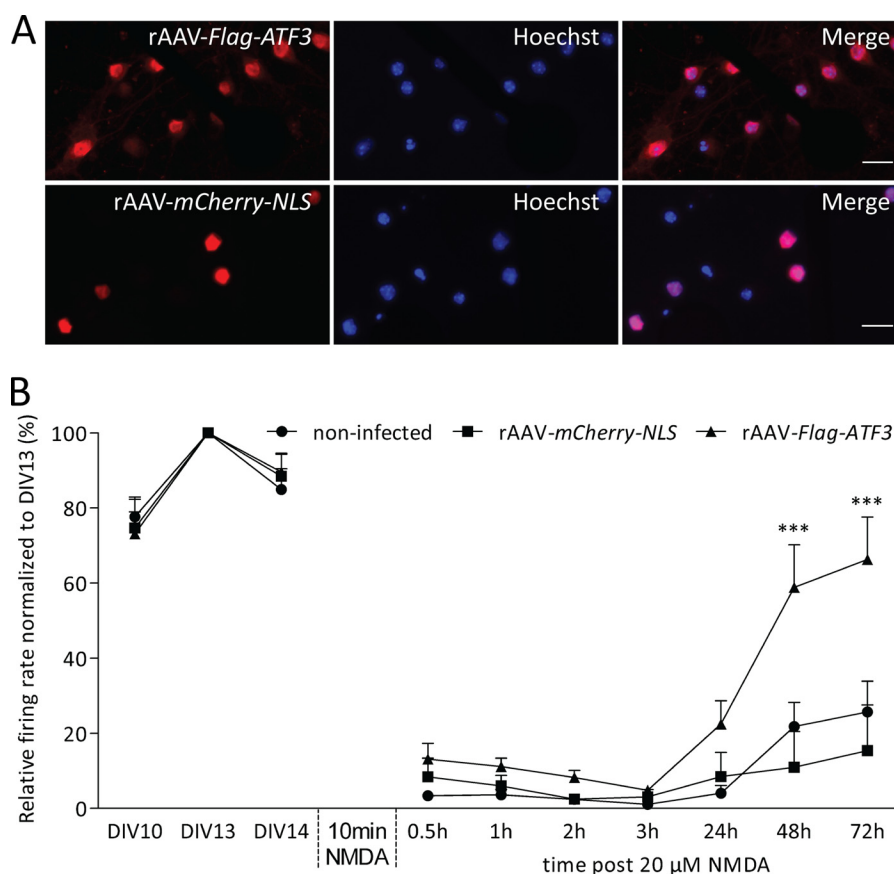


FIGURE 6. **ATF3-mediated dendroprotection enhances recovery of neuronal network activity after an excitotoxic insult.** *A* and *B*, for MEA analysis, hippocampal neurons were infected at DIV7 with either rAAV-ATF3-FLAG or with rAAV-mCherry-NLS. Representative images of rAAV-ATF3-FLAG-infected hippocampal neurons labeled with anti-FLAG antibody (*upper panels*) and rAAV-NLS-mCherry infected hippocampal neurons (*lower panels*) plated on MEAs. Scale bars, 20 μ m (*A*). Firing rates were normalized to their respective rates at DIV13 of uninfected hippocampal neurons and hippocampal neurons infected with rAAV-ATF3-FLAG or rAAV-mCherry-NLS at the indicated time points before and after a 10-min application of 20 μ M NMDA (*B*). Statistically significant differences are indicated with asterisks as follows: ***, $p < 0.001$. Data are presented as mean + S.E.

to be involved in initial dendritic beading (30, 53). However, both dendritic beading and microtubule fragmentation are prevented by pretreatment with the microtubule-stabilizing compound taxol (34, 53–56). These findings suggest that both the initial disruption of microtubule morphology and dendritic beading may result from excessive water influx.

Excessive influx of water and cell swelling compromises the health of neurons. During ischemia, both neurons and astrocytes swell. Although astrocytes tend to survive such an insult, possibly as a result of their ability to rapidly recover from swelling (43, 57), neurons often die. The balancing of cellular water content in astrocytes is most likely facilitated by plasma membrane aquaporin water channels (58, 59). In contrast, hippocampal neurons are not known to express any functional membrane-bound aquaporins (39). Indeed, even the route for water entry into hippocampal neurons is not clear. The plasma membrane of hippocampal neurons is largely water-impermeable at resting membrane potential and resists volume changes under acute osmotic stress (60); yet neurons swell rapidly during conditions of prolonged depolarization and during brain ischemia (39, 43). Water is thought to follow the initial sodium/chloride influx (32), although no candidate water channels have been suggested for the possible route of entry, and the majority of sodium and chloride ions are stripped from their hydration

shell before entering the cell (61). One possibility is that, during pathophysiological conditions, water enters through large pore channels possibly involved in maintaining anoxic depolarization (39, 62). Alternatively, as neurons are resistant to passive water transport under physiological conditions, water may enter via a secondary active transport mechanism, such as ion exchangers.

AP Bursting Protects Mitochondria and Dendrites against Excitotoxic Damage—Permanent dendritic beading depends on a large increase in the intracellular calcium concentration (30, 63) followed by the breakdown of the mitochondrial membrane potential (37, 64). Calcium entry into neurons during excitotoxicity occurs via eNMDARs and causes the activation of transcriptional shut-off pathways, calcium flux into mitochondria, mitochondrial dysfunction, and dendritic beading (5, 6, 65, 66). In contrast, sNMDARs promote cell survival (16–19) and, as shown in this study, protect against acute dendrotoxicity. Synaptic activity and sNMDAR stimulation can both delay and reduce the magnitude of NMDA-induced loss of mitochondrial membrane potential (26). Therefore, one possibility is that the protection against dendritic beading and facilitated recovery following synaptic activity observed here may be a consequence of an increased resistance of mitochondria to excitotoxic stimuli. Calcium may enter mitochondria also fol-

ATF3 Protects against Dendrotoxicity

lowing stimulation of sNMDARs, which triggers the dissociation of mitochondria from microtubules and their subsequent recruitment to synapses (38). Therefore, increased synaptic activity may cause mitochondria to move physically away from eNMDARs, thereby reducing the likelihood that toxic levels of calcium entering through eNMDARs flow into mitochondria.

ATF3 Protects against Dendrotoxicity—Increased synaptic activity controls a pool of nuclear calcium- and CREB-regulated genes, which include *ATF3* (17, 19, 20). This study revealed that *ATF3* protects against dendritic beading and, more importantly, that it allows neurons to regain functional connections after an excitotoxic challenge. To minimize the damage after a brain injury and maximize the potential for functional recovery, it is important to maintain or restore neuronal function at an early stage of damage to sustain synaptic activity and its survival-promoting effects.

The exact mechanism by which ATF3 attenuates dendrotoxicity and enhances cell survival is unknown. It acts as a transcriptional repressor and may, directly or indirectly, cause changes in the expression of genes involved in microtubule stabilization or water influx. Consistent with its possible role in microtubule stabilization is the observation that ATF3 contributes to nerve regeneration by promoting neurite outgrowth after nerve injury both *in vitro* and *in vivo* (48, 49, 67).

Implications for the Development of Novel Dendroprotective Therapies—The development of clinically effective neuroprotective agents can be improved by broadening the spectrum of parameters used to assess neuronal damage in *in vitro* studies. Many studies evaluate merely cell death rates but lack information on changes in neuronal network functions. Because the restoration of synaptic transmission of damaged yet alive neurons following a brain injury is important, *in vitro* studies should combine cell death analyses with the assessment of additional morphological and functional parameters, such as the characterization of dendrite morphology and synaptic transmission. Using this approach, we could demonstrate that ATF3 offers not only protection against apoptotic and necrotic cell death (17, 19, 20) but also reduces dendrotoxicity and enhances the recovery of synaptic connectivity after an excitotoxic insult. Identification of ATF3 target genes that mediate these activities is likely to provide an important lead in the search for an effective dendroprotective therapy to attenuate brain injury-associated neuronal network dysfunction and loss of neurons.

Acknowledgments—We thank Iris Bünzli-Ehret for help with the preparation of hippocampal cultures and Anna M. Hertle and David Lau for the construction of a rAAV expressing mitochondrially targeted mCherry.

REFERENCES

- Lipton, S. A., and Rosenberg, P. A. (1994) Excitatory amino acids as a final common pathway for neurologic disorders. *N. Engl. J. Med.* **330**, 613–622
- Katsura, K., Kristián, T., and Siesjö, B. K. (1994) Energy metabolism, ion homeostasis, and cell damage in the brain. *Biochem. Soc. Trans.* **22**, 991–996
- Olney, J. W. (1969) Brain lesions, obesity, and other disturbances in mice treated with monosodium glutamate. *Science* **164**, 719–721
- Dirnagl, U., Iadecola, C., and Moskowitz, M. A. (1999) Pathobiology of ischaemic stroke: an integrated view. *Trends Neurosci.* **22**, 391–397
- Hardingham, G. E., Fukunaga, Y., and Bading, H. (2002) Extrasynaptic NMDARs oppose synaptic NMDARs by triggering CREB shut-off and cell death pathways. *Nat. Neurosci.* **5**, 405–414
- Hardingham, G. E., and Bading, H. (2010) Synaptic versus extrasynaptic NMDA receptor signalling: implications for neurodegenerative disorders. *Nat. Rev. Neurosci.* **11**, 682–696
- Olney, J. W., Fuller, T., and de Gubareff, T. (1979) Acute dendrotoxic changes in the hippocampus of kainate-treated rats. *Brain Res.* **176**, 91–100
- Hori, N., and Carpenter, D. O. (1994) Functional and morphological changes induced by transient *in vivo* ischemia. *Exp. Neurol.* **129**, 279–289
- von Lubitz, D. K., and Diemer, N. H. (1983) Cerebral ischemia in the rat: ultrastructural and morphometric analysis of synapses in stratum radiatum of the hippocampal CA-1 region. *Acta Neuropathol.* **61**, 52–60
- Risher, W. C., Ard, D., Yuan, J., and Kirov, S. A. (2010) Recurrent spontaneous spreading depolarizations facilitate acute dendritic injury in the ischemic penumbra. *J. Neurosci.* **30**, 9859–9868
- Risher, W. C., Lee, M. R., Fomitcheva, I. V., Hess, D. C., and Kirov, S. A. (2011) Dibucaine mitigates spreading depolarization in human neocortical slices and prevents acute dendritic injury in the ischemic rodent neocortex. *PLoS One* **6**, e22351
- Enright, L. E., Zhang, S., and Murphy, T. H. (2007) Fine mapping of the spatial relationship between acute ischemia and dendritic structure indicates selective vulnerability of layer V neuron dendritic tufts within single neurons *in vivo*. *J. Cereb. Blood Flow Metab.* **27**, 1185–1200
- Murphy, T. H., Li, P., Betts, K., and Liu, R. (2008) Two-photon imaging of stroke onset *in vivo* reveals that NMDA-receptor independent ischemic depolarization is the major cause of rapid reversible damage to dendrites and spines. *J. Neurosci.* **28**, 1756–1772
- Sigler, A., and Murphy, T. H. (2010) *In vivo* 2-photon imaging of fine structure in the rodent brain: before, during, and after stroke. *Stroke* **41**, S117–S123
- Zhang, S., Boyd, J., Delaney, K., and Murphy, T. H. (2005) Rapid reversible changes in dendritic spine structure *in vivo* gated by the degree of ischemia. *J. Neurosci.* **25**, 5333–5338
- Papadia, S., Stevenson, P., Hardingham, N. R., Bading, H., and Hardingham, G. E. (2005) Nuclear Ca^{2+} and the cAMP response element-binding protein family mediate a late phase of activity-dependent neuroprotection. *J. Neurosci.* **25**, 4279–4287
- Zhang, S. J., Zou, M., Lu, L., Lau, D., Ditzel, D. A., Delucinge-Vivier, C., Aso, Y., Descombes, P., and Bading, H. (2009) Nuclear calcium signaling controls expression of a large gene pool: identification of a gene program for acquired neuroprotection induced by synaptic activity. *PLoS Genet.* **5**, e1000604
- Lee, B., Butcher, G. Q., Hoyt, K. R., Impy, S., and Obrietan, K. (2005) Activity-dependent neuroprotection and cAMP response element-binding protein (CREB): Kinase coupling, stimulus intensity, and temporal regulation of CREB phosphorylation at serine 133. *J. Neurosci.* **25**, 1137–1148
- Zhang, S. J., Steijaert, M. N., Lau, D., Schütz, G., Delucinge-Vivier, C., Descombes, P., and Bading, H. (2007) Decoding NMDA receptor signaling: Identification of genomic programs specifying neuronal survival and death. *Neuron* **53**, 549–562
- Zhang, S. J., Buchthal, B., Lau, D., Hayer, S., Dick, O., Schwaninger, M., Veltkamp, R., Zou, M., Weiss, U., and Bading, H. (2011) A signaling cascade of nuclear calcium-CREB-ATF3 activated by synaptic NMDA receptors defines a gene repression module that protects against extrasynaptic NMDA receptor-induced neuronal cell death and ischemic brain damage. *J. Neurosci.* **31**, 4978–4990
- Bading, H., and Greenberg, M. E. (1991) Stimulation of protein tyrosine phosphorylation by NMDA receptor activation. *Science* **253**, 912–914
- Soriano, F. X., Papadia, S., Hofmann, F., Hardingham, N. R., Bading, H., and Hardingham, G. E. (2006) Preconditioning doses of NMDA promote neuroprotection by enhancing neuronal excitability. *J. Neurosci.* **26**, 4509–4518
- Arnold, F. J., Hofmann, F., Bengtson, C. P., Wittmann, M., Vanhoutte, P., and Bading, H. (2005) Microelectrode array recordings of cultured hippocampal networks reveal a simple model for transcription and protein

- synthesis-dependent plasticity. *J. Physiol.* **564**, 3–19
24. Bading, H., Ginty, D. D., and Greenberg, M. E. (1993) Regulation of gene expression in hippocampal neurons by distinct calcium signaling pathways. *Science* **260**, 181–186
 25. Wiegert, J. S., Bengtson, C. P., and Bading, H. (2007) Diffusion and not active transport underlies and limits ERK1/2 synapse-to-nucleus signaling in hippocampal neurons. *J. Biol. Chem.* **282**, 29621–29633
 26. Lau, D., and Bading, H. (2009) Synaptic activity-mediated suppression of p53 and induction of nuclear calcium-regulated neuroprotective genes promote survival through inhibition of mitochondrial permeability transition. *J. Neurosci.* **29**, 4420–4429
 27. Klugmann, M., Symes, C. W., Leichtlein, C. B., Klaussner, B. K., Dunning, J., Fong, D., Young, D., and During, M. J. (2005) AAV-mediated hippocampal expression of short and long Homer 1 proteins differentially affect cognition and seizure activity in adult rats. *Mol. Cell. Neurosci.* **28**, 347–360
 28. Tauskela, J. S., Comas, T., Hewitt, K., Monette, R., Paris, J., Hogan, M., and Morley, P. (2001) Cross-tolerance to otherwise lethal *N*-methyl-D-aspartate and oxygen-glucose deprivation in preconditioned cortical cultures. *Neuroscience* **107**, 571–584
 29. Reynolds, E. S. (1963) The use of lead citrate at high pH as an electron-opaque stain in electron microscopy. *J. Cell Biol.* **17**, 208–212
 30. Faddis, B. T., Hasbani, M. J., and Goldberg, M. P. (1997) Calcipain activation contributes to dendritic remodeling after brief excitotoxic injury *in vitro*. *J. Neurosci.* **17**, 951–959
 31. Ikegaya, Y., Kim, J. A., Baba, M., Iwatsubo, T., Nishiyama, N., and Matsuki, N. (2001) Rapid and reversible changes in dendrite morphology and synaptic efficacy following NMDA receptor activation: implication for a cellular defense against excitotoxicity. *J. Cell Sci.* **114**, 4083–4093
 32. Hasbani, M. J., Hyrc, K. L., Faddis, B. T., Romano, C., and Goldberg, M. P. (1998) Distinct roles for sodium, chloride, and calcium in excitotoxic dendritic injury and recovery. *Exp. Neurol.* **154**, 241–258
 33. Hasbani, M. J., Schlieff, M. L., Fisher, D. A., and Goldberg, M. P. (2001) Dendritic spines lost during glutamate receptor activation reemerge at original sites of synaptic contact. *J. Neurosci.* **21**, 2393–2403
 34. Park, J. S., Bateman, M. C., and Goldberg, M. P. (1996) Rapid alterations in dendrite morphology during sublethal hypoxia or glutamate receptor activation. *Neurobiol. Dis.* **3**, 215–227
 35. Brewer, L. D., Thibault, O., Staton, J., Thibault, V., Rogers, J. T., Garcia-Ramos, G., Kraner, S., Landfield, P. W., and Porter, N. M. (2007) Increased vulnerability of hippocampal neurons with age in culture: temporal association with increases in NMDA receptor current, NR2A subunit expression, and recruitment of L-type calcium channels. *Brain Res.* **1151**, 20–31
 36. Rintoul, G. L., Filiano, A. J., Brocard, J. B., Kress, G. J., and Reynolds, I. J. (2003) Glutamate decreases mitochondrial size and movement in primary forebrain neurons. *J. Neurosci.* **23**, 7881–7888
 37. Greenwood, S. M., Mizielinska, S. M., Frenguelli, B. G., Harvey, J., and Connolly, C. N. (2007) Mitochondrial dysfunction and dendritic beading during neuronal toxicity. *J. Biol. Chem.* **282**, 26235–26244
 38. Macaskill, A. F., Rinholm, J. E., Twelvetrees, A. E., Arancibia-Carcamo, I. L., Muir, J., Fransson, A., Aspenstrom, P., Attwell, D., and Kittler, J. T. (2009) Miro1 is a calcium sensor for glutamate receptor-dependent localization of mitochondria at synapses. *Neuron* **61**, 541–555
 39. Andrew, R. D., Labron, M. W., Boehnke, S. E., Carnduff, L., and Kirov, S. A. (2007) Physiological evidence that pyramidal neurons lack functional water channels. *Cereb. Cortex* **17**, 787–802
 40. Li, P., and Murphy, T. H. (2008) Two-photon imaging during prolonged middle cerebral artery occlusion in mice reveals recovery of dendritic structure after reperfusion. *J. Neurosci.* **28**, 11970–11979
 41. Petito, C. K., and Pulsinelli, W. A. (1984) Delayed neuronal recovery and neuronal death in rat hippocampus following severe cerebral ischemia: possible relationship to abnormalities in neuronal processes. *J. Cereb. Blood Flow Metab.* **4**, 194–205
 42. Hasbani, M. J., Viquez, N. M., and Goldberg, M. P. (2001) NMDA receptors mediate hypoxic spine loss in cultured neurons. *Neuroreport* **12**, 2731–2735
 43. Risher, W. C., Andrew, R. D., and Kirov, S. A. (2009) Real-time passive volume responses of astrocytes to acute osmotic and ischemic stress in cortical slices and *in vivo* revealed by two-photon microscopy. *Glia* **57**, 207–221
 44. Bengtson, C. P., Dick, O., and Bading, H. (2008) A quantitative method to assess extrasynaptic NMDA receptor function in the protective effect of synaptic activity against neurotoxicity. *BMC Neurosci.* **9**, 11
 45. Papadia, S., Soriano, F. X., Léveillé, F., Martel, M. A., Dakin, K. A., Hansen, H. H., Kaindl, A., Sifringer, M., Fowler, J., Stefovská, V., McKenzie, G., Craigon, M., Corriveau, R., Ghazal, P., Horsburgh, K., Yankner, B. A., Wyllie, D. J., Ikonomidou, C., and Hardingham, G. E. (2008) Synaptic NMDA receptor activity boosts intrinsic antioxidant defenses. *Nat. Neurosci.* **11**, 476–487
 46. Buchs, P. A., and Muller, D. (1996) Induction of long-term potentiation is associated with major ultrastructural changes of activated synapses. *Proc. Natl. Acad. Sci. U.S.A.* **93**, 8040–8045
 47. Wang, J., Campos, B., Jamieson, G. A., Jr., Kaetzel, M. A., and Dedman, J. R. (1995) Functional elimination of calmodulin within the nucleus by targeted expression of an inhibitor peptide. *J. Biol. Chem.* **270**, 30245–30248
 48. Seiffers, R., Allchorne, A. J., and Woolf, C. J. (2006) The transcription factor ATF-3 promotes neurite outgrowth. *Mol. Cell. Neurosci.* **32**, 143–154
 49. Seiffers, R., Mills, C. D., and Woolf, C. J. (2007) ATF3 increases the intrinsic growth state of DRG neurons to enhance peripheral nerve regeneration. *J. Neurosci.* **27**, 7911–7920
 50. Matesic, D. F., and Lin, R. C. (1994) Microtubule-associated protein 2 as an early indicator of ischemia-induced neurodegeneration in the gerbil forebrain. *J. Neurochem.* **63**, 1012–1020
 51. Dreier, J. P. (2011) The role of spreading depression, spreading depolarization and spreading ischemia in neurological disease. *Nat. Med.* **17**, 439–447
 52. Schliwa, M., Euteneuer, U., Bulinski, J. C., and Izant, J. G. (1981) Calcium lability of cytoplasmic microtubules and its modulation by microtubule-associated proteins. *Proc. Natl. Acad. Sci. U.S.A.* **78**, 1037–1041
 53. Hoskison, M. M., and Shuttleworth, C. W. (2006) Microtubule disruption, not calcipain-dependent loss of MAP2, contributes to enduring NMDA-induced dendritic dysfunction in acute hippocampal slices. *Exp. Neurol.* **202**, 302–312
 54. Emery, D. G., and Lucas, J. H. (1995) Ultrastructural damage and neuritic beading in cold-stressed spinal neurons with comparisons to NMDA and A23187 toxicity. *Brain Res.* **692**, 161–173
 55. Furukawa, K., and Mattson, M. P. (1995) Taxol stabilizes $[Ca^{2+}]_i$ and protects hippocampal neurons against excitotoxicity. *Brain Res.* **689**, 141–146
 56. Tseng, C. Y., and Firestein, B. L. (2011) The role of PSD-95 and cypin in morphological changes in dendrites following sublethal NMDA exposure. *J. Neurosci.* **31**, 15468–15480
 57. Pekny, M., and Nilsson, M. (2005) Astrocyte activation and reactive gliosis. *Glia* **50**, 427–434
 58. Amiry-Moghaddam, M., and Ottersen, O. P. (2003) The molecular basis of water transport in the brain. *Nat. Rev. Neurosci.* **4**, 991–1001
 59. Nielsen, S., Nagelhus, E. A., Amiry-Moghaddam, M., Bourque, C., Agre, P., and Ottersen, O. P. (1997) Specialized membrane domains for water transport in glial cells: High-resolution immunogold cytochemistry of aquaporin-4 in rat brain. *J. Neurosci.* **17**, 171–180
 60. Somjen, G. G., Faas, G. C., Vreugdenhil, M., and Wadman, W. J. (1993) Channel shutdown: A response of hippocampal neurons to adverse environments. *Brain Res.* **632**, 180–194
 61. MacAulay, N., and Zeuthen, T. (2010) Water transport between CNS compartments: Contributions of aquaporins and cotransporters. *Neuroscience* **168**, 941–956
 62. Anderson, T. R., Jarvis, C. R., Biedermann, A. J., Molnar, C., and Andrew, R. D. (2005) Blocking the anoxic depolarization protects without functional compromise following simulated stroke in cortical brain slices. *J. Neurophysiol.* **93**, 963–979
 63. Vander Jagt, T. A., Connor, J. A., and Shuttleworth, C. W. (2008) Localized loss of Ca^{2+} homeostasis in neuronal dendrites is a downstream consequence of metabolic compromise during extended NMDA exposures. *J. Neurosci.* **28**, 5029–5039
 64. Kintner, D. B., Chen, X., Currie, J., Chanana, V., Ferrazzano, P., Baba, A.,

ATF3 Protects against Dendrotoxicity

- Matsuda, T., Cohen, M., Orlowski, J., Chiu, S. Y., Taunton, J., and Sun, D. (2010) Excessive Na^+/H^+ exchange in disruption of dendritic Na^+ and Ca^{2+} homeostasis and mitochondrial dysfunction following *in vitro* ischemia. *J. Biol. Chem.* **285**, 35155–35168
65. Dick, O., and Bading, H. (2010) Synaptic activity and nuclear calcium signaling protect hippocampal neurons from death signal-associated nuclear translocation of FoxO3a induced by extrasynaptic *N*-methyl-D-aspartate receptors. *J. Biol. Chem.* **285**, 19354–19361
66. Léveillé, F., El Gaamouch, F., Gouix, E., Lecocq, M., Lobner, D., Nicole, O., and Buisson, A. (2008) Neuronal viability is controlled by a functional relation between synaptic and extrasynaptic NMDA receptors. *FASEB J.* **22**, 4258–4271
67. Nakagomi, S., Suzuki, Y., Namikawa, K., Kiryu-Seo, S., and Kiyama, H. (2003) Expression of the activating transcription factor 3 prevents c-Jun N-terminal kinase-induced neuronal death by promoting heat shock protein 27 expression and Akt activation. *J. Neurosci.* **23**, 5187–5196